arXiv:astro-ph/9712150v1 11 Dec 1997

On the difficulty of launching an outflow from an accretion disk

Gordon I. Ogilvie[1] and Mario Livio[2]

Space Telescope Science Institute, 3700 San Martin Drive, Baltimore, MD 21218

Received _____; accepted _____

Accepted for publication in the *Astrophysical Journal*

[1]Permanent address: Institute of Astronomy, University of Cambridge, Madingley Road, Cambridge CB3 0HA, United Kingdom. e-mail address: gogilvie@ast.cam.ac.uk

[2]e-mail address: mlivio@stsci.edu

ABSTRACT

We solve for the local vertical structure of a thin accretion disk threaded by a poloidal magnetic field. The angular velocity deviates from the Keplerian value as a result of the radial Lorentz force, but is constant on magnetic surfaces. Angular momentum transport and energy dissipation in the disk are parametrized by an α-prescription, and a Kramers opacity law is assumed to hold. We also determine the stability of the equilibria with respect to the magnetorotational (or Balbus–Hawley) instability. If the magnetic field is sufficiently strong, stable equilibria can be found in which the angle of inclination, i, of the magnetic field to the vertical at the surface of the disk has any value in the range $0 \leq i < 90°$. By analyzing the dynamics of a transonic outflow in the corona of the disk, we show that a certain potential difference must be overcome even when $i > 30°$. We determine this potential difference as a function of i for increasing values of the vertical magnetic field strength. For magnetorotationally stable equilibria, the potential difference increases faster than the fourth power of the magnetic field strength, quickly exceeding a value corresponding to the central temperature of the disk, and is minimized with respect to i at $i \approx 38°$. We show that this property is relatively insensitive to the form of the opacity law. Our results suggest that an additional source of energy, such as coronal heating, may be required for the launching of an outflow from a magnetized disk.

Subject headings: accretion, accretion disks — hydrodynamics — MHD

1. Introduction

The highly collimated outflows associated with many astrophysical objects, from young stellar objects to active galactic nuclei, are widely believed to originate in accretion disks threaded by magnetic fields (see, e.g., Livio 1997 for a recent review). While winds from rotating stars such as the Sun are influenced by magnetohydrodynamic (MHD) effects, in particular with regard to the magnetic braking of the star (e.g. Mestel 1968), these outflows are driven predominantly by thermal effects in the corona of the star. In the case of accretion disks, however, the possibility arises of a wind driven predominantly by dynamical effects.

The influential model of Blandford & Payne (1982) established the significance of the angle of inclination, i, of the poloidal magnetic field lines to the vertical at the surface of the disk. They showed that, when $i > 30°$, an outflow is driven spontaneously by the centrifugal force (as viewed in the frame of reference rotating at the local Keplerian angular velocity). This effect occurs because, for material forced to rotate at the angular velocity of the foot-point of the magnetic field line, the centrifugal–gravitational potential decreases, rather than increases, along the field line leaving the surface of the disk.

This result should not be interpreted as meaning that a wind can flow freely and steadily from the surface of the disk without any thermal assistance. If that were possible, it would lead to the dynamical disruption of the entire disk, and it would be more correct to say that the disk was never in equilibrium to begin with. Blandford & Payne (1982) appreciated that their model of a 'cold' wind does not properly describe the flow in the neighborhood of the surface of the disk, where thermal effects must become important. Indeed, the flow must pass through a sonic (strictly, slow magnetosonic) point in this region and can do so only with thermal assistance. The purpose of our investigation is to determine quantitatively how much assistance is required.

We are interested in the internal equilibrium of the disk and in the properties of the wind in the region immediately above the surface of the disk. It is therefore sufficient to consider a radially localized region of the disk and solve for its vertical structure. The present work is most closely related to that of Wardle & Königl (1993), who applied a similar procedure to weakly ionized, protostellar disks in which ambipolar diffusion is important. There are several significant differences in our approach, however, which are described in detail at the end of this paper.

In several other studies (e.g. Cao & Spruit 1994; Lubow, Papaloizou, & Pringle 1994; Kudoh & Shibata 1997), the shape and angular velocity of the magnetic field lines is assumed, but we determine them self-consistently by solving the relevant equations. Another approach used recently (e.g. Ouyed & Pudritz 1997) is to solve for the wind flow in the corona of the disk using axisymmetric numerical simulations. We emphasize that, since these simulations describe the flow only *after* it has become supersonic, they are complementary to, but quite distinct from, the present work.

Recently, Livio (1997) reviewed the observations of all the classes of astrophysical objects with which jets are associated. Working on the assumption that the same mechanism of acceleration and collimation operates in all these systems, he argued that the most probable such mechanism is indeed the predominantly centrifugally driven MHD wind described above. He also suggested that an additional source of energy is required to produce jets that are sufficiently powerful to be observed. In this paper, we will provide qualitative and quantitative evidence in support of this hypothesis.

It is now well established that weakly magnetized accretion disks are subject to a magnetorotational instability (Velikhov 1959; Chandrasekhar 1960; Balbus & Hawley 1991) of which the non-linear development is a state of MHD turbulence (Brandenburg et al. 1995; Hawley, Gammie, & Balbus 1995; Stone et al. 1996). For this reason, we include a

stability analysis as part of this investigation. However, we do not attempt to address the precise relation between MHD turbulence and MHD winds.

The remainder of this paper is organized as follows. In §2, we present the equations governing the equilibrium of the disk, and describe the numerical solutions in terms of 'standard', dimensionless units. We also discuss the stability of the equilibria. In §3, we consider the dynamics of a transonic outflow in the corona of the disk, and identify the potential difference that must be overcome by such an outflow. In §4, we translate the results into physical units. Finally, in §5, we discuss the implications of our analysis, with an emphasis on cataclysmic variable (CV) systems.

2. Equilibrium of the disk

2.1. Basic equations

In this section we describe the local vertical structure of a magnetized accretion disk such as might be found in a CV system. The disk is taken to be a steady, axisymmetric MHD flow in the gravitational potential of a spherical mass M. The usual cylindrical polar coordinates (r, ϕ, z) are adopted. In the limit of a geometrically thin disk, the governing equations may be simplified considerably by means of an asymptotic analysis (Ogilvie 1997a; hereafter, Paper I) in which the small parameter ϵ is a characteristic value of $H(r)/r$, where $z = H(r)$ is the location of the upper surface of the disk at radius r. They then take the form of ordinary differential equations (ODEs) in the vertical coordinate z at each radius r separately, which describe the local vertical equilibrium of the disk. There is also an integral relation describing the global magnetic structure, but here we are concerned only with the local aspects of the problem.

In the present work we do not repeat the formal asymptotic analysis, but present

the simplified, approximate equations that result from it. The dynamical aspects of the equilibrium were considered in Paper I, but the treatment of thermal and radiative physics below is new.[3] We consider the equations below to afford a minimal description of the problem while allowing quantitative predictions to be made.

2.1.1. Balance of forces

The angular velocity of the fluid is written as $\Omega = \Omega_0 + \Omega_1$, where

$$\Omega_0 = \left(\frac{GM}{r^3}\right)^{1/2} \tag{1}$$

is the Keplerian value, which is independent of z, and Ω_1 is the deviation from Keplerian rotation, which depends on z, but is much smaller than Ω_0. The radial component of the momentum equation then becomes

$$-2\rho r\Omega_0\Omega_1 = \frac{B_z}{\mu_0}\frac{\partial B_r}{\partial z}. \tag{2}$$

(We write the permeability of free space as μ_0, but will substitute $\mu_0 = 4\pi$ later for calculations in CGS units.) This equation states that the radial tension force associated with the bending magnetic field produces the deviation from Keplerian rotation. Radial gradients of fluid and magnetic pressures are negligible, as are the inertial effects of the accretion flow. The vertical component of the momentum equation is

$$0 = -\frac{\partial p}{\partial z} - \frac{B_r}{\mu_0}\frac{\partial B_r}{\partial z} - \rho\Omega_0^2 z. \tag{3}$$

This equation states that both the pressure of the radial magnetic field and the vertical gravitational force act to compress the disk. The pressure of any toroidal magnetic field is neglected, as is the self-gravitation of the disk.

[3]The scalings correspond to the 'weakly magnetized disks' of Paper I, although equilibria resembling the 'strongly magnetized disks' will appear in the limit of a strong magnetic field.

2.1.2. Magnetic field

The solenoidal condition on the magnetic field implies

$$\frac{\partial B_z}{\partial z} = 0. \tag{4}$$

The induction equation reduces to the condition of isorotation, $\mathbf{B}\cdot\nabla\Omega = 0$, which becomes

$$-\frac{3\Omega_0}{2r}B_r + B_z\frac{\partial\Omega_1}{\partial z} = 0. \tag{5}$$

The effects of any turbulence in the disk on the *mean* magnetic field are neglected. If the scale of the turbulent motions were small compared to the scale on which the magnetic field varies, it might be possible to describe the mean turbulent EMF in terms of an α-effect, representing the regeneration of the mean magnetic field, and a β-effect, representing turbulent diffusion (e.g. Moffatt 1978). However, there is no such separation of scales in the present problem and the effects of any turbulence are completely uncertain. Although these effects may be important in practice, our assumption of isorotation is the simplest way to proceed in the face of this uncertainty.

2.1.3. Thermal and radiative physics

Instead of prescribing a polytropic relation between pressure and density, as was done in Paper I, we now include thermal and radiative physics. The disk is assumed to be optically thick, with Rosseland mean opacity κ. The vertical radiative energy flux is then

$$F = -\frac{16\sigma T^3}{3\kappa\rho}\frac{\partial T}{\partial z}, \tag{6}$$

and the energy equation may be written

$$\frac{\partial F}{\partial z} = \frac{3}{2}\Omega_0\sigma_{r\phi}, \tag{7}$$

where $\sigma_{r\phi}$ is the component of the stress tensor responsible for angular momentum transport and dissipation of energy. (Note that the solutions we are considering are stable against convection.)

For a complete specification of the problem, an equation of state must be supplied, and also prescriptions for the opacity and stress. We use the ideal gas law,

$$p = \frac{k\rho T}{\mu m_{\rm H}}, \tag{8}$$

where μ is the mean molecular weight of the gas. This assumes that the radiation pressure is negligible. For the stress, we adopt the conventional α-prescription,

$$\sigma_{r\phi} = \alpha p, \tag{9}$$

where α is a constant. For the opacity, we assume a Kramers law,

$$\kappa = \kappa_0 \rho T^{-7/2}, \tag{10}$$

where κ_0 is a constant. This is an adequate approximation when free-free absorption is the dominant source of opacity, as is usually the case in CV disks. We consider more general opacity laws in §4 below. While equation (9) represents the most uncertain element of this treatment, it does allow a comparison to be made with previous work.

2.1.4. Boundary conditions

We solve the equations in $0 < z < H$, and apply symmetry conditions

$$B_r = 0 \tag{11}$$

and

$$F = 0 \tag{12}$$

at $z = 0$. The magnetic field then has dipolar symmetry. The boundary conditions at $z = H$ are taken to be

$$\rho = 0, \tag{13}$$

$$T = 0 \tag{14}$$

and

$$B_r = B_z \tan i, \tag{15}$$

where i is the angle of inclination of the magnetic field to the vertical at the surface of the disk.

2.1.5. Conservation of angular momentum

A further relation, which allows quantities to be expressed in terms of the accretion rate $\dot{M}$, is obtained from the conservation of angular momentum. Making the usual assumptions about the nature of the boundary layer near the surface of the central object at radius r_* (e.g. Pringle 1981), we obtain

$$r^2 \Omega_0 f \dot{M} = 2\pi r^2 \int \sigma_{r\phi} \, \mathrm{d}z, \tag{16}$$

where

$$f = 1 - \left(\frac{r_*}{r} \right)^{1/2}. \tag{17}$$

Then

$$F_\mathrm{s} = \frac{3}{8\pi} \Omega_0^2 f \dot{M}, \tag{18}$$

where the subscript 's' denotes the value at the surface of the disk.

This is one equation in which a toroidal magnetic field might have a significant effect. If the disk has an outflow which exerts a torque comparable to that due to $\sigma_{r\phi}$, it can be considered to increase the effective value of F_s in this equation. However, it is assumed that

the rate at which mass is lost to the wind is small compared to $\dot{M}$. (See, e.g., Livio 1997 for observational evidence suggesting that this is indeed the case.)

2.2. Transformation of the equations

We now recast the equations in dimensionless form by means of the following transformations.

$$z = \tilde{z}\, H, \tag{19}$$

$$\Omega_1 = \tilde{\Omega}_1 \left(\frac{H}{r}\right) \Omega_0, \tag{20}$$

$$\rho = \tilde{\rho} \left(\frac{3\alpha}{2}\right)^{-1/3} H^{11/3} \Omega_0^4 \left(\frac{\mu m_{\rm H}}{k}\right)^{5/2} \left(\frac{16\sigma}{3\kappa_0}\right)^{1/3}, \tag{21}$$

$$p = \tilde{p} \left(\frac{3\alpha}{2}\right)^{-1/3} H^{17/3} \Omega_0^6 \left(\frac{\mu m_{\rm H}}{k}\right)^{5/2} \left(\frac{16\sigma}{3\kappa_0}\right)^{1/3}, \tag{22}$$

$$\mathbf{B} = \tilde{\mathbf{B}} \left(\frac{3\alpha}{2}\right)^{-1/6} \mu_0^{1/2} H^{17/6} \Omega_0^3 \left(\frac{\mu m_{\rm H}}{k}\right)^{5/4} \left(\frac{16\sigma}{3\kappa_0}\right)^{1/6}, \tag{23}$$

$$T = \tilde{T}\, H^2 \Omega_0^2 \left(\frac{\mu m_{\rm H}}{k}\right), \tag{24}$$

$$F = \tilde{F} \left(\frac{3\alpha}{2}\right)^{2/3} H^{20/3} \Omega_0^7 \left(\frac{\mu m_{\rm H}}{k}\right)^{5/2} \left(\frac{16\sigma}{3\kappa_0}\right)^{1/3}. \tag{25}$$

The dimensionless equations are

$$\frac{\partial \tilde{\Omega}_1}{\partial \tilde{z}} = \frac{3\tilde{B}_r}{2\tilde{B}_z}, \tag{26}$$

$$\frac{\partial \tilde{p}}{\partial \tilde{z}} = -\tilde{\rho}\tilde{z} + \frac{2\tilde{\rho}\tilde{\Omega}_1 \tilde{B}_r}{\tilde{B}_z}, \tag{27}$$

$$\frac{\partial \tilde{B}_r}{\partial \tilde{z}} = -\frac{2\tilde{\rho}\tilde{\Omega}_1}{\tilde{B}_z}, \tag{28}$$

$$\frac{\partial \tilde{T}}{\partial \tilde{z}} = -\tilde{\rho}^2 \tilde{T}^{-13/2} \tilde{F}, \tag{29}$$

$$\frac{\partial \tilde{F}}{\partial \tilde{z}} = \tilde{p}, \tag{30}$$

$$\tilde{p} = \tilde{\rho}\tilde{T}. \tag{31}$$

We then have a fifth-order system of non-linear ODEs on $0 < \tilde{z} < 1$, with boundary conditions

$$\tilde{B}_r(0) = 0, \tag{32}$$

$$\tilde{F}(0) = 0, \tag{33}$$

$$\tilde{\rho}(1) = 0, \tag{34}$$

$$\tilde{T}(1) = 0, \tag{35}$$

$$\tilde{B}_r(1) = \tilde{B}_z \tan i, \tag{36}$$

and with two dimensionless parameters, $\tilde{B}_z$ and i, which may be taken to be non-negative without loss of generality. Note that the dimensionless viscosity parameter α has been scaled out of the equations. We remark that a similar reduction of the equations could be made for any equation of state, stress prescription and opacity law that are 'simple', in the sense of being monomials of the thermodynamic variables.

Dimensionless variables written with tildes will be said to be expressed in 'standard' units. These units allow the simplest and most natural presentation of the equations and their solutions. They are based on the length scale H, the time scale Ω^{-1}, and mass and temperature scales derived from the coefficients appearing in the equation of state and the opacity law; they also incorporate the scalings of the solutions with H/r and α. However, since H is not known a priori, a further transformation is made in §4 below to express quantities in 'physical' units based on the accretion rate. For this reason, the interpretation of numerical results in the next section should be regarded as provisional. The final interpretation is offered in §4.

2.3. Numerical solutions

An expansion of the required solution of equations (26)–(31) in powers of $(1 - \tilde{z})$ is readily obtained which allows the equations to be integrated smoothly out of the singular point $\tilde{z} = 1$ towards $\tilde{z} = 0$. Shooting is then required in two dimensions to match the symmetry conditions on $\tilde{z} = 0$. As discussed by Ogilvie (1997b), for certain values of the parameters there exist solutions in which the magnetic field bends more than once as it passes through the disk. Such 'irregular' equilibria are known to be unstable and are not discussed here. The regular equilibria occupy a connected region in the parameter space, as shown in Figure 1. The edge of this region has a form similar to that obtained for polytropic disks. Equilibria with any angle $i < 30^\circ$ exist for any value of $\tilde{B}_z$, but angles $i > 30^\circ$ can be achieved only if the magnetic field is sufficiently strong. As the edge of the solution manifold is approached, the effective gravitational acceleration parallel to the magnetic field at the surface of the disk tends to zero, which in a time-dependent situation would lead to the dynamical disruption of the disk.

EDITOR: PLACE FIGURE 1 HERE.

The equilibria exhibit a wide variety of behavior in different parts of the parameter space, and certain features of this should be explained. First, when $i = 0$, the equilibria are unaffected by the magnetic field and all take the form of the unmagnetized solution. Secondly, when i is fixed, with $0 < i < 30^\circ$, and the limit $\tilde{B}_z \to 0$ is taken, the equilibria eventually become physically unrealistic. Much of the disk becomes almost evacuated, with mass concentrated near the equatorial plane and near the surface. This behavior is the only way to prevent the magnetic field lines from bending many times as they pass through the disk, when the field is very weak. While these equilibria are almost certainly unstable to overturning, this behavior occurs only when they are already unstable to the

magnetorotational instability, as described in §2.4 below. Thirdly, when i is fixed, with $i > 0$, and the limit $\tilde{B}_z \to \infty$ is taken, the equilibria approach a strongly magnetized limit in which they are compressed only by the Lorentz force and not by gravity. We find the asymptotic form of the solution to be

$$\tilde{\Omega}_1(\tilde{z}) = -\tilde{B}_z^{12/19}(\tan i)^{-7/19}\,\lambda + O(1), \tag{37}$$

$$\tilde{\rho}(\tilde{z}) \sim (\tilde{B}_z \tan i)^{26/19}\, y_1(\tilde{z}), \tag{38}$$

$$\tilde{p}(\tilde{z}) \sim (\tilde{B}_z \tan i)^{2}\, y_2(\tilde{z}), \tag{39}$$

$$\tilde{B}_r(\tilde{z}) \sim (\tilde{B}_z \tan i)\, y_3(\tilde{z}), \tag{40}$$

$$\tilde{T}(\tilde{z}) \sim (\tilde{B}_z \tan i)^{12/19}\, y_4(\tilde{z}), \tag{41}$$

$$\tilde{F}(\tilde{z}) \sim (\tilde{B}_z \tan i)^{2}\, y_5(\tilde{z}), \tag{42}$$

where λ is an eigenvalue of the non-linear system

$$y_2' = -2\lambda y_1 y_3, \tag{43}$$

$$y_3' = 2\lambda y_1, \tag{44}$$

$$y_4' = -y_1^2 y_4^{-13/2} y_5, \tag{45}$$

$$y_5' = y_2, \tag{46}$$

$$y_2 = y_1 y_4, \tag{47}$$

with boundary conditions

$$y_3(0) = 0, \tag{48}$$

$$y_5(0) = 0, \tag{49}$$

$$y_1(1) = 0, \tag{50}$$

$$y_4(1) = 0, \tag{51}$$

$$y_3(1) = 1. \tag{52}$$

Here, a prime denotes differentiation with respect to the argument. The numerically determined solution is $\lambda \approx 1.916$. Also required is the quantity $y_5(1) \approx 0.1607$. This limiting behavior of the equilibria is used in §4 below.

The plasma beta, being the ratio of the gas pressure to the magnetic pressure, is often taken to be a dimensionless, inverse measure of the strength of the magnetic field. However, as explained in Paper I, this is not appropriate in the case of strongly magnetized accretion disks. In the limit $\tilde{B}_z \to \infty$, the plasma beta, evaluated on the equatorial plane, tends to a constant value which depends on i. This is because the nature of the vertical equilibrium in the strongly magnetized limit requires that the gas pressure increase in proportion to the magnetic pressure.

2.4. Magnetorotational stability of the equilibria

If the magnetic field is sufficiently weak, the equilibria are expected to be unstable to the magnetorotational instability (Balbus & Hawley 1991). The instability of a thin disk containing a bending poloidal magnetic field has been analyzed by Ogilvie (1997b), who found that the curve of marginal stability in the parameter space could be located by solving the equations for an equilibrium possessing a mode with zero frequency and zero radial wavenumber. In terms of the Lagrangian displacement ξ, these are

$$3\Omega_0^2 \rho\, \xi_r = -B_z \frac{\partial}{\partial z}\left(B_z \frac{\partial \xi_r}{\partial z} - B_r \frac{\partial \xi_z}{\partial z} \right) \tag{53}$$

and

$$\Omega_0^2 z \frac{\partial \rho}{\partial z}\, \xi_z = \frac{\partial\, \delta\Pi}{\partial z} - \rho \Omega_0^2 z \frac{\partial \xi_z}{\partial z}, \tag{54}$$

where

$$\delta\Pi = \rho \Omega_0^2 z\, \xi_z + B_r B_z \frac{\partial \xi_r}{\partial z} - (\gamma p + B_r^2) \frac{\partial \xi_z}{\partial z} \tag{55}$$

is the Eulerian perturbation of total pressure. This assumes that the perturbations are adiabatic, with adiabatic exponent γ. The relevant mode is the first mode of odd symmetry, which satisfies the boundary conditions

$$\xi_r = \frac{\partial \xi_z}{\partial z} = 0 \tag{56}$$

at $z = 0$, and

$$\frac{\partial \xi_r}{\partial z} - \tan i \, \frac{\partial \xi_z}{\partial z} = 0 \tag{57}$$

at $z = H$. The dimensionless form of these equations is identical except for the inclusion of the tildes and the omission of Ω_0.

The curve of marginal stability, for the case $\gamma = 5/3$, is shown in Figure 2. Again, this is qualitatively similar to curves obtained for polytropic disks.

EDITOR: PLACE FIGURE 2 HERE.

As discussed by Ogilvie (1997b), it is expected that the equilibria that are stable to the magnetorotational instability are also stable to the magnetoconvective (Parker), interchange, and bending instabilities, unless the magnetic field provides most of the support against the radial gravitational force. Although a weak, global, non-axisymmetric instability may remain, this is unlikely to be dynamically important in a thin disk.

3. Dynamics of an outflow in the corona of the disk

Following Paper I, we now analyze the dynamics of a transonic outflow in the region immediately above the disk, which we refer to as the 'corona', and which is defined by $H < z \ll r$. The density of the wind is very much smaller than that of the disk, possibly by a factor $O(\epsilon^4)$, and to match the solutions in detail would require high-order asymptotics

well beyond the scope of this analysis. Instead, we consider that the disk acts as a reservoir which can supply any reasonable mass flux to the wind, the corresponding velocity field required in the disk being extremely small.

In the corona, the magnetic field is force-free to a very good approximation, and the field lines are straight on the length scale H. They act as rigid channels for the wind and also enforce isorotation. The dynamics of the outflow in this region depends critically on the centrifugal–gravitational potential $\Phi^{\rm cg}$, which may be computed as follows. Since the magnetic field is force-free, $\partial B_r/\partial z = 0$, so that $B_r = B_z \tan i$ throughout the corona. Equation (5) may then be integrated to give

$$\Omega_1 = \Omega_{1\rm s} + \frac{3\Omega_0 (z - H) \tan i}{2r}, \tag{58}$$

where, again, the subscript 's' denotes the value at the surface of the disk. The effective gravitational acceleration is

$$\mathbf{g} = 2r\Omega_0\Omega_1\, \mathbf{e}_r - \Omega_0^2 z\, \mathbf{e}_z, \tag{59}$$

and its component measured parallel to the magnetic field (and towards the surface of the disk) is

$$g_\parallel = -(3\tan^2 i - 1)\Omega_0^2 (z - H)\cos i + \Omega_0(\Omega_0 H - 2\Omega_{1\rm s} r \tan i)\cos i. \tag{60}$$

If, as we assume, $i > 30^\circ$, then $g_\parallel$ decreases linearly with increasing z and goes to zero at $z = z_{\rm sonic}$, given by

$$z_{\rm sonic} = H + \frac{(\Omega_0 H - 2\Omega_{1\rm s} r \tan i)}{(3\tan^2 i - 1)\Omega_0}. \tag{61}$$

This name is appropriate because, as shown below, $z = z_{\rm sonic}$ is the expected location of the sonic point of a transonic wind. Consider a single magnetic field line, and let z parametrize the position along it. When $g_\parallel$ is integrated along the field line, it yields the centrifugal–gravitational potential

$$\Phi^{\rm cg} = -\tfrac{1}{2}(3\tan^2 i - 1)\Omega_0^2 (z - z_{\rm sonic})^2, \tag{62}$$

as measured from the sonic point. In particular, the potential difference between the sonic point and the surface of the disk is

$$\Delta\Phi = \frac{(\Omega_0 H - 2\Omega_{1s} r \tan i)^2}{2(3\tan^2 i - 1)}. \tag{63}$$

When i approaches 30° (from above), the height of the sonic point increases without bound, as does the potential difference. However, these expressions are valid only if the height of the sonic point calculated from equation (61) satisfies $z_{\rm sonic} \ll r$, since otherwise the quadratic approximation to the potential ceases to be valid and the curvature of the magnetic field lines should also be taken into account. Within this approximation, the potential difference is always small compared to GM/r. (By comparison, when $i < 30°$, the potential difference is comparable to GM/r.)

We now consider the dynamics of a transonic wind flowing along the magnetic field lines. The wind is treated as isothermal, since the optical depth is presumably small in the corona, and therefore

$$p = c^2 \rho, \tag{64}$$

where

$$c = \left(\frac{kT}{\mu m_{\rm H}}\right)^{1/2} \tag{65}$$

is the isothermal sound speed. Mass conservation requires that the mass flux density

$$\rho u = \mathcal{F} = \text{constant} \tag{66}$$

be constant along the flow. The Bernoulli equation states that

$$\tfrac{1}{2}u^2 + c^2 \ln\rho + \Phi^{\rm cg} = \text{constant} \tag{67}$$

is also constant following the flow. On differentiating this equation we obtain

$$(u^2 - c^2)\frac{{\rm d}\ln u}{{\rm d}z} = (3\tan^2 i - 1)\Omega_0^2 (z - z_{\rm sonic}), \tag{68}$$

which demonstrates that the sonic transition must occur at $z = z_{\rm sonic}$. In terms of the Mach number $\mathcal{M} = u/c$, we then have

$$\tfrac{1}{2}(\mathcal{M}^2 - 1) - \ln \mathcal{M} = -\Phi^{\rm cg}/c^2, \tag{69}$$

and, in particular,

$$\tfrac{1}{2}(\mathcal{M}_{\rm s}^2 - 1) - \ln \mathcal{M}_{\rm s} = \Delta\Phi/c^2 \tag{70}$$

is a transcendental equation for the Mach number $\mathcal{M}_{\rm s}$ at the surface of the disk. The mass flux density is then

$$\mathcal{F} = \mathcal{M}_{\rm s}\rho_{\rm s}c, \tag{71}$$

where $\rho_{\rm s}$ is the density of the wind at the surface of the disk. When $\Delta\Phi \gg c^2$, an approximate solution is

$$\mathcal{M}_{\rm s} \approx \exp(-\Delta\Phi/c^2 - \tfrac{1}{2}), \tag{72}$$

which implies

$$\mathcal{F} \approx \rho_{\rm s}c\, \exp(-\Delta\Phi/c^2 - \tfrac{1}{2}). \tag{73}$$

The numerical solution of equation (70) in Figure 3 shows that this approximation is accurate even for moderate values of $\Delta\Phi/c^2$.

EDITOR: PLACE FIGURE 3 HERE.

Evidently the meaning of equation (73) is that the outflow is severely choked if the potential difference is much larger than c^2. For any equilibrium we can compute $\Delta\Phi$ and deduce the sound speed – and therefore the temperature – required in the corona for the outflow not to be suppressed. The height of the sonic point and the potential difference are plotted as functions of i for various values of $\tilde{B}_z$ in Figure 4. These equilibria are all stable to the magnetorotational instability. As i increases from 30°, the sonic point approaches the surface of the disk and the potential difference decreases, until the equilibrium ceases to

exist. When the magnetic field is stronger, the sonic point is more distant and the potential difference is larger. However, for any field strength, an angle i can be found for which the potential difference is arbitrarily small. In the next section we show that this property is lost when the solutions are expressed in more physical units which take account of the compression of the disk by the magnetic field.

EDITOR: PLACE FIGURE 4 HERE.

4. The solutions expressed in physical units

4.1. Definition of units

Although the dimensionless forms defined in §2.2 are convenient for the purposes of computation, one would like to express the magnetic field, for example, in units of gauss rather than in the dimensionless form $\tilde{\mathbf{B}}$. The relation between $\mathbf{B}$ and $\tilde{\mathbf{B}}$ involves H which is not known a priori. However, the accretion rate $\dot{M}$ is determined a priori in the sense of being of a global property of the disk, independent of radius, whose value can be estimated observationally. From the numerical solutions, we know $\tilde{F}_{\rm s}$ for each equilibrium, which allows us to write

$$\frac{3}{8\pi}\Omega_0^2 f\dot{M} = \tilde{F}_{\rm s}\left(\frac{3\alpha}{2}\right)^{2/3} H^{20/3}\Omega_0^7\left(\frac{\mu m_{\rm H}}{k}\right)^{5/2}\left(\frac{16\sigma}{3\kappa_0}\right)^{1/3}, \tag{74}$$

combining equations (18) and (25). We then have

$$H = \tilde{F}_{\rm s}^{-3/20}\, U_H, \tag{75}$$

where

$$U_H = \left(\frac{3}{8\pi}\right)^{3/20}\left(\frac{3\alpha}{2}\right)^{-1/10}\Omega_0^{-3/4}\left(\frac{\mu m_{\rm H}}{k}\right)^{-3/8}\left(\frac{16\sigma}{3\kappa_0}\right)^{-1/20} f^{3/20}\dot{M}^{3/20} \tag{76}$$

is a suitable unit of length. Similarly, we may write

$$\mathbf{B} = \tilde{\mathbf{B}} \tilde{F}_{\rm s}^{-17/40} \, U_B \tag{77}$$

and

$$T = \tilde{T} \tilde{F}_{\rm s}^{-3/10} \, U_T, \tag{78}$$

where

$$U_B = \left(\frac{3}{8\pi}\right)^{17/40} \left(\frac{3\alpha}{2}\right)^{-9/20} \mu_0^{1/2} \Omega_0^{7/8} \left(\frac{\mu m_{\rm H}}{k}\right)^{3/16} \left(\frac{16\sigma}{3\kappa_0}\right)^{1/40} f^{17/40} \dot{M}^{17/40} \tag{79}$$

and

$$U_T = \left(\frac{3}{8\pi}\right)^{3/10} \left(\frac{3\alpha}{2}\right)^{-1/5} \Omega_0^{1/2} \left(\frac{\mu m_{\rm H}}{k}\right)^{1/4} \left(\frac{16\sigma}{3\kappa_0}\right)^{-1/10} f^{3/10} \dot{M}^{3/10} \tag{80}$$

are suitable units of magnetic field strength and of temperature.

In terms of CGS units, we find

$$U_H \approx 1.2 \times 10^8 \, \alpha^{-1/10} M_1^{-3/8} R_{10}^{9/8} f^{3/20} \dot{M}_{16}^{3/20} \, {\rm cm}, \tag{81}$$

$$U_B \approx 1.0 \times 10^3 \, \alpha^{-9/20} M_1^{7/16} R_{10}^{-21/16} f^{17/40} \dot{M}_{16}^{17/40} \, {\rm gauss}, \tag{82}$$

$$U_T \approx 1.3 \times 10^4 \, \alpha^{-1/5} M_1^{1/4} R_{10}^{-3/4} f^{3/10} \dot{M}_{16}^{3/10} \, {\rm K}, \tag{83}$$

where $M_1 = M/M_\odot$, $R_{10} = R/(10^{10}\,{\rm cm})$, $\dot{M}_{16} = \dot{M}/(10^{16}\,{\rm g\,s^{-1}})$, and we have used the values $\mu \approx 0.6$ and $\kappa_0 \approx 6.4 \times 10^{22}\,{\rm cm^2\,g^{-1}}$ (cf. Novikov & Thorne 1973) appropriate for CV disks.

4.2. Solutions with a purely vertical magnetic field

When the magnetic field is purely vertical, it does not affect the equilibrium. The solution is the same for all values of $\tilde{B}_z$, and is found numerically to have $\tilde{F}_{\rm s} \approx 0.0007041$. We then obtain

$$H \approx 2.971 \, U_H \approx 3.5 \times 10^8 \, \alpha^{-1/10} M_1^{-3/8} R_{10}^{9/8} f^{3/20} \dot{M}_{16}^{3/20} \, {\rm cm}. \tag{84}$$

We note that this is larger by a factor of approximately 2 than the value quoted by, for example, Frank, King, & Raine (1985), which was based on order-of-magnitude estimates (although we define H to be the true semi-thickness rather than an approximate scale height). The magnetic field strength for marginal magnetorotational stability is found to be $\tilde{B}_z \approx 0.06327$, or

$$B_z \approx 1.383\, U_B \approx 1.4 \times 10^3\, \alpha^{-9/20} M_1^{7/16} R_{10}^{-21/16} f^{17/40} \dot{M}_{16}^{17/40}\, \mathrm{gauss}. \tag{85}$$

If the magnetic field results from the aligned dipole field of a central white dwarf of radius $5.0 \times 10^8\,\mathrm{cm}$, a value of $1.4 \times 10^3\,\mathrm{gauss}$ at a radius of $10^{10}\,\mathrm{cm}$ in the disk would correspond to a value of $2.2 \times 10^7\,\mathrm{gauss}$ at the poles of the white dwarf. This means that the disk would be unstable at this radius in many cases of astrophysical interest, but may be stable in some systems such as V1500 Cyg.

4.3. Solutions with an inclined magnetic field

We now redraw Figure 2 in physical units, using $\tilde{B}_z \tilde{F}_\mathrm{s}^{-17/40}$ as the ordinate rather than $\tilde{B}_z$. Unfortunately the resulting graph (Figure 5), while more physically meaningful, is more difficult to interpret. The mapping from $\tilde{B}_z$ to $\tilde{B}_z \tilde{F}_\mathrm{s}^{-17/40}$ is not one-to-one, with the result that the solution manifold folds over on itself on the left-hand side of Figure 5. However, the 'folded' solutions are unstable and this detail need not be pursued here. More interesting is the way in which the curve on which the equilibria cease to exist is transformed relative to Figure 2. This distortion occurs because equilibria with highly inclined magnetic field lines are strongly compressed by the Lorentz force and therefore have a higher pressure than the unmagnetized solution with the same H. The stress and torque are correspondingly increased, so that $\tilde{F}_\mathrm{s}$ is large, and therefore B_z/U_B is smaller than might be expected.

EDITOR: PLACE FIGURE 5 HERE.

The existence of the fold means that, when the magnetic field strength is reduced below the stability boundary, the equilibria eventually cease to exist. However, it is of little importance whether, in this part of the parameter space, no stable solution exists or no solution whatever exists. The result is likely to be a state of MHD turbulence.

The height of the sonic point and the potential difference, expressed in physical units, are plotted as functions of i for various values of B_z/U_B in Figure 6. The height of the sonic point is compared with H, both expressed in units of U_H. For the potential difference we introduce a physical unit

$$U_\Phi = \frac{kU_T}{\mu m_{\rm H}} \approx 1.8 \times 10^{12}\, \alpha^{-1/5} M_1^{1/4} R_{10}^{-3/4} f^{3/10} \dot{M}_{16}^{3/10}\, {\rm cm}^2\, {\rm s}^{-2}. \tag{86}$$

Then $\Delta\Phi/U_\Phi$ can be compared with $T_{\rm c}/U_T$, where $T_{\rm c}$ is the central temperature of the disk.

EDITOR: PLACE FIGURE 6 HERE.

In the range $1.55 \lesssim B_z/U_B \lesssim 1.93$, there exist stable equilibria such that, when i is increased from 30°, the potential difference falls rapidly from infinity to zero as the sonic point approaches the surface of the disk, and then the equilibria cease to exist. This behavior is similar to the interpretation offered earlier, based on Figure 4 and standard units. There are also equilibria with more highly inclined magnetic field lines. However, for $B_z/U_B \gtrsim 1.93$, a different behavior is found. As i is increased from 30°, the equilibria continue to exist for all angles up to 90°. The potential difference has a minimum, typically in the range $38° \lesssim i \lesssim 43°$, and then increases again. The sonic point at first approaches the surface of the disk, but then recedes from it. Moreover, as B_z/U_B is increased, the minimum potential difference increases very rapidly and quickly exceeds a value corresponding to the central temperature of the disk.

4.4. Limiting behavior for strongly magnetized disks

When B_z/U_B is sufficiently large, the limiting form of the equilibria given in §2.3 applies. We then find that the potential difference is

$$\frac{\Delta\Phi}{U_\Phi} \sim C_1 \left(\frac{B_z}{U_B}\right)^{84/19} \frac{(\tan i)^{84/19}}{(3\tan^2 i - 1)}, \tag{87}$$

where

$$C_1 = 2\lambda^2 [y_5(1)]^{30/19} \approx 0.4095. \tag{88}$$

This increases very rapidly with increasing magnetic field strength. The minimum with respect to i occurs at

$$i = \arctan\sqrt{\frac{14}{23}} \approx 37.96^\circ. \tag{89}$$

Similarly, the height of the sonic point is

$$\frac{z_{\rm sonic}}{U_H} \sim C_2 \left(\frac{B_z}{U_B}\right)^{42/19} \frac{(\tan i)^{42/19}}{(3\tan^2 i - 1)}, \tag{90}$$

where

$$C_2 = 2\lambda [y_5(1)]^{15/19} \approx 0.9050, \tag{91}$$

and this has a minimum with respect to i at

$$i = \arctan\sqrt{\frac{7}{2}} \approx 74.05^\circ. \tag{92}$$

To show that these power laws and characteristic angles are relatively insensitive to the opacity law, the analysis can be repeated using a more general relation of the form

$$\kappa = \kappa_0 \rho^x T^y. \tag{93}$$

We then find that the potential difference is

$$\frac{\Delta\Phi}{U_\Phi} \sim C_1 \left(\frac{B_z}{U_B}\right)^{4(5+2x-y)/(5+x-y)} \frac{(\tan i)^{4(5+2x-y)/(5+x-y)}}{(3\tan^2 i - 1)}, \tag{94}$$

where C_1 depends on x and y, and of course the units U_Φ, U_B, etc., are differently but analogously defined. This shows that the potential difference typically scales as approximately the fourth power of the magnetic field strength. The minimum with respect to i occurs at

$$i = \arctan\sqrt{\frac{2(5+2x-y)}{3(5+3x-y)}}, \tag{95}$$

provided that

$$\frac{5+3x-y}{5+x-y} > 0. \tag{96}$$

Similarly, the height of the sonic point is

$$\frac{z_{\rm sonic}}{U_H} \sim C_2 \left(\frac{B_z}{U_B}\right)^{2(5+2x-y)/(5+x-y)} \frac{(\tan i)^{2(5+2x-y)/(5+x-y)}}{(3\tan^2 i - 1)}, \tag{97}$$

and this has a minimum with respect to i at

$$i = \arctan\sqrt{\frac{5+2x-y}{3x}}, \tag{98}$$

provided that

$$\frac{x}{5+x-y} > 0. \tag{99}$$

Criterion (96) is satisfied for most reasonable opacity laws, as shown in Figure 7. In the case of electron-scattering opacity, for which $x = y = 0$, the potential difference scales as $(B_z/U_B)^4$ and is minimized with respect to i at $i \approx 39.23°$. Criterion (99) marginally fails to be satisfied, however, so that the height of the sonic point continues to decrease as i approaches 90°.

EDITOR: PLACE FIGURE 7 HERE.

In Figure 8 we compare the true minimum of the potential difference with respect to i with the value predicted from equation (87). This shows that the limiting behavior described in this section is achieved very rapidly as the vertical magnetic field strength is increased beyond the stability boundary.

EDITOR: PLACE FIGURE 8 HERE.

5. Discussion

In this paper we have solved for the local vertical structure of a magnetized accretion disk such as might be found in a CV system. The magnetic field was assumed to enforce isorotation, and the deviation from Keplerian rotation was taken fully into account. Angular momentum transport in the disk was parametrized by an α-prescription in the conventional way, and a Kramers opacity law was assumed to hold. We have shown that, when quantities are expressed in physical units, equilibria that are magnetorotationally stable can be found in which the angle of inclination, i, of the magnetic field to the vertical at the surface of the disk has any value in the range $0 \leq i < 90^\circ$ if the magnetic field is sufficiently strong.

We have analyzed the dynamics of a transonic outflow in the corona of the disk when $i > 30^\circ$, and, in particular, have shown that a certain potential difference must be overcome by such an outflow. When the equilibria are very close to the magnetorotational stability boundary, the potential difference is relatively small and can in fact be made arbitrarily small by approaching the edge of the solution manifold. For more strongly magnetized disks, however, *the potential difference increases faster than the fourth power of the magnetic field strength, and is minimized with respect to i at $i \approx 38^\circ$*. These properties are relatively insensitive to the opacity law.

We have used a local representation which neglects the global form of the disk and wind, focusing instead on the vertical structure at a single radius. In this respect our analysis is comparable with that of Wardle & Königl (1993). However, in the limit in which ambipolar diffusion is negligible, as is the case in the accretion disks of many classes of objects such as CVs, no meaningful solution of their equations can be obtained, even though

some of their equations correspond in this limit to the ones we have solved. To insist that the disk achieves a balance between the outward diffusion of magnetic flux and its inward advection by the accretion flow is certainly attractive, but constrains the problem in such a way that it appears that diffusion is driving the outflow.

Certain other features of our analysis should be emphasized. First, we do *not* assume that the wind accounts for all, or even most, of the angular momentum transport in the disk. In the case of CV disks, for example, we can be confident that the agent supplying most of the torque on the disk is not an MHD wind; see the discussion by Livio (1997). Secondly, we consider the disk to have a well-defined surface which is hardly affected by the presence or absence of an outflow above it. We do not attempt to make a smooth transition between the disk and the wind, except in requiring the continuity of the mass and magnetic fluxes, because the density of the wind is so small that a detailed matching procedure would require high-order asymptotics. Thirdly, we do not consider ambipolar diffusion, Ohmic resistivity or turbulent diffusion of the magnetic field. Instead, we assume that isorotation holds on magnetic field lines and we allow for a slow accretion of magnetic flux by the disk. Finally, we have considered an optically thick disk rather than assuming the disk to be isothermal. We note that, if the disk is isothermal, it is easier to obtain an outflow of reasonable strength without postulating a hot corona, because the region above the disk always has the same temperature as the central temperature.

The interpretation of our results depends to some extent on the class of accretion disks under consideration, and on the source of the mean magnetic field. In the case of CV disks, for example, the magnetic field of the white dwarf can be important and may be sufficient to make at least the inner part of the disk magnetorotationally stable (cf. eq. [85]). In that case, even if the magnetic field lines are inclined such that $i > 30^\circ$, our results suggest that the potential difference may be too large to allow a significant outflow unless the

disk has a hot corona or access to an additional source of energy, such as nuclear burning, in accordance with the hypothesis of Livio (1997). However, the interaction between a magnetized central object and the disk may be more complicated than we have allowed for in this paper (cf. Livio & Pringle 1992; Miller & Stone 1997). In other cases, magnetic flux may be accreted from the environment or may be a remnant of the formation of the disk. In disks that are magnetorotationally unstable, the dynamics of the mean magnetic field is much less certain, but it may be possible for these systems to regulate the distribution of magnetic flux so as to remain close to the stability limit, and thereby avoid incurring a very large potential difference.

GIO thanks the Space Telescope Science Institute for its hospitality. ML acknowledges support from NASA Grant NAGW-2678.

REFERENCES

Balbus, S. A., & Hawley, J. F. 1991, ApJ, 376, 214

Blandford, R. D., & Payne, D. G. 1982, MNRAS, 199, 883

Brandenburg, A., Nordlund, Å., Stein, R. F., & Torkelsson, U. 1995, ApJ, 446, 741

Cao, X., & Spruit, H. C. 1994, A&A, 287, 80

Chandrasekhar, S. 1960, Proc. Natl Acad. Sci., 46, 253

Frank, J., King, A. R., & Raine, D. J. 1985, Accretion Power in Astrophysics (Cambridge: Cambridge Univ. Press)

Hawley, J. F., Gammie, C. F., & Balbus, S. A. 1995, ApJ, 440, 742

Kudoh, T., & Shibata, K. 1997, ApJ, 474, 362

Livio, M. 1997, in Accretion Phenomena and Related Outflows, ed. D. T. Wickramasinghe, G. V. Bicknell, & L. Ferrario (San Francisco: ASP Conf. Ser.), 845

Livio, M., & Pringle, J. E. 1992, MNRAS, 259, 23P

Lubow, S. H., Papaloizou, J. C. B., & Pringle, J. E. 1994, MNRAS, 268, 1010

Mestel, L. 1968, MNRAS, 138, 359

Miller, K. A., & Stone, J. M. 1997, ApJ, 489, 890

Moffatt, H. K. 1978, Magnetic Field Generation in Electrically Conducting Fluids (Cambridge: Cambridge Univ. Press)

Novikov, I. D., & Thorne, K. S. 1973, in Black Holes, ed. C. DeWitt & B. S. DeWitt (New York: Gordon & Breach), 343

Ogilvie, G. I. 1997a, MNRAS, 288, 63 (Paper I)

Ogilvie, G. I. 1997b, MNRAS, submitted

Ouyed, R., & Pudritz, R. E. 1997, ApJ, 482, 712

Pringle, J. E. 1981, ARA&A, 19, 137

Stone, J. M., Hawley, J. F., Gammie, C. F., & Balbus, S. A. 1996, ApJ, 463, 656

Velikhov, E. P. 1959, Sov. Phys. JETP, 9, 995

Wardle, M., & Königl, A. 1993, ApJ, 410, 218

This manuscript was prepared with the AAS LaTeX macros v4.0.

Fig. 1.— Parameter space of equilibrium solutions. $\tilde{B}_z$ is the vertical magnetic field in the disk, expressed in standard units (eq. [23]), and i is the angle of inclination of the magnetic field to the vertical at the surface of the disk. *Dashed line*: edge of the solution manifold; regular equilibria exist everywhere to the left of this line. *Dotted line*: drawn at an angle $i = 30°$, which is critical to the analysis in §3. (In this graph only, a logarithmic scale of magnetic field strength is used in order to give a broad perspective on the parameter space.)

Fig. 2.— *Solid line*: stability boundary to the magnetorotational instability, for the case $\gamma = 5/3$. *Dashed line*: edge of the solution manifold, as in Figure 1. (Note that the axes are quite different from those of Figure 1.)

Fig. 3.— Dependence of the Mach number $\mathcal{M}_{\rm s}$ of the wind at the surface of the disk on the potential difference $\Delta\Phi$ between the sonic point and the surface, expressed in units of c^2, where c is the isothermal sound speed. The solid line denotes the true solution, while the dashed line represents the approximation given in equation (72).

Fig. 4.— Variation with i of the height of the sonic point (a) and the potential difference between the sonic point and the surface (b), both expressed in standard units, for equilibria with $\tilde{B}_z = 0.1$ (*solid line*), 0.2 (*dotted line*) and 0.3 (*dashed line*).

Fig. 5.— Parameter space with the vertical magnetic field B_z expressed in physical units (eq. [79]). *Solid line*: stability boundary. *Dashed line*: edge of the solution manifold. *Dot-dashed line*: fold in the solution manifold. No regular equilibria are found below a curve which consists of the dot-dashed line continued by the dashed line.

Fig. 6.— *Panels a, c, and e*: height of the sonic point (*solid line*) compared with H (*dotted line*), both expressed in physical units, as functions of i, for equilibria with $B_z/U_B = 1.8$ (a), 2.0 (c), and 3.0 (e). *Panels b, d, and f*: potential difference (*solid line*) compared with the central temperature (*dotted line*), both expressed in physical units, for equilibria with

$B_z/U_B = 1.8$ (b), 2.0 (d), and 3.0 (f). Note the different scale for the potential difference and temperature in panel f.

Fig. 7.— Parameter space of opacity laws $\kappa = \kappa_0 \rho^x T^y$. The points marked 'K' and 'ES' correspond to Kramers opacity and electron-scattering opacity, respectively. *Solid lines*: contours of the angle of inclination for which the potential difference is minimized when expressed in physical units (eq. [95]). The contour values are 31°, 32°, ..., 40°. *Dotted lines*: contours equivalent to 30° and 90°; in the narrow sector between these lines, a minimum is not obtained.

Fig. 8.— *Solid line*: true minimum of the potential difference with respect to i, as a function of the vertical magnetic field strength, both expressed in physical units. *Dotted line*: the limiting form calculated from equation (87).

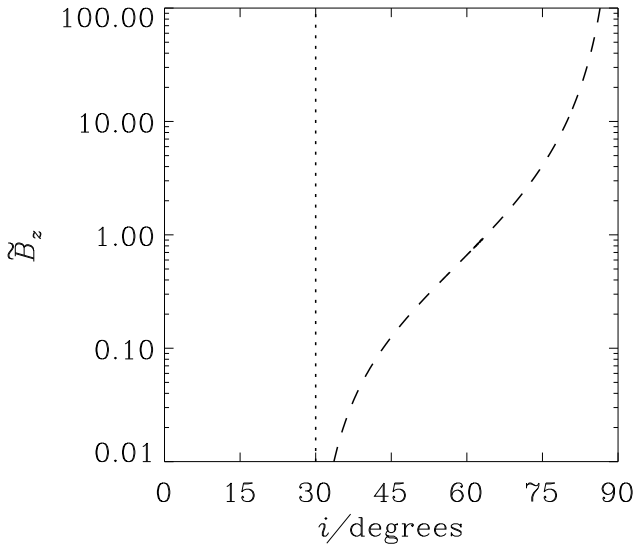
100.00
10.00
1.00
0.10
0.01
$\widetilde{B}_z$
0
15
30
45
60
75
90
i/degrees

Figure 1

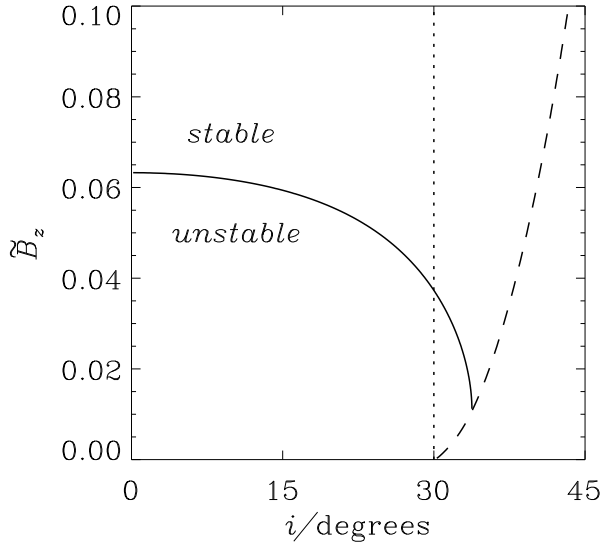
0.10
0.08
0.06
0.04
0.02
0.00
stable
unstable
$\widetilde{B}_z$
0
15
30
45
i/degrees

Figure 2

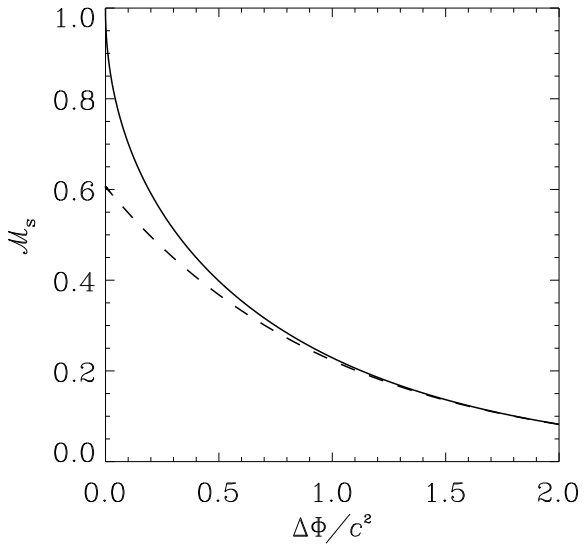

Figure 3

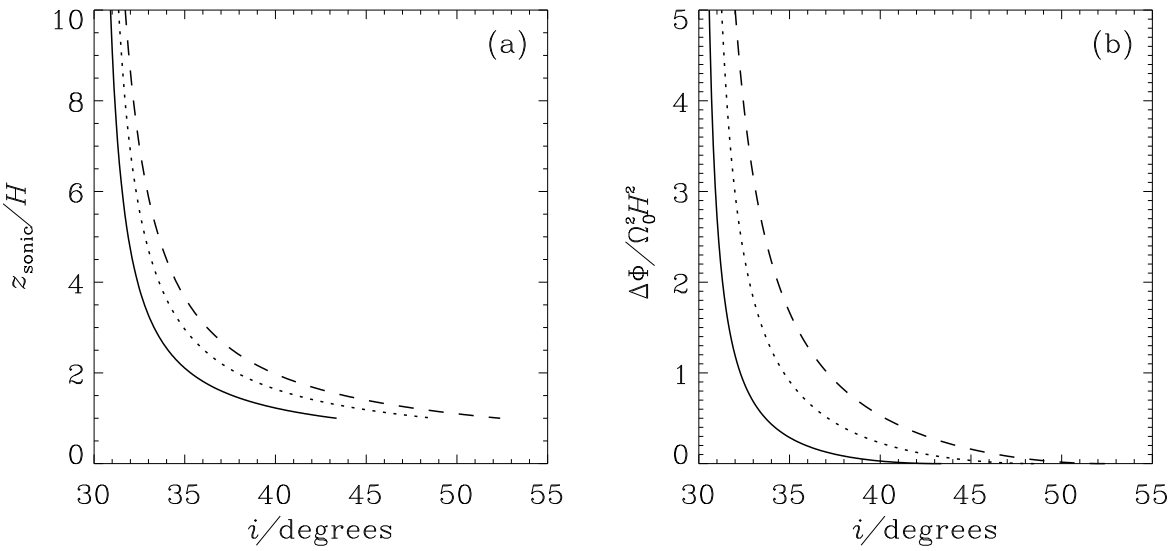
(a)
(b)
$z_{\rm sonic}/H$
$\Delta\Phi/\Omega_0^2 H^2$
i/degrees
i/degrees
0
2
4
6
8
10
1
3
5
30
35
40
45
50
55

Figure 4

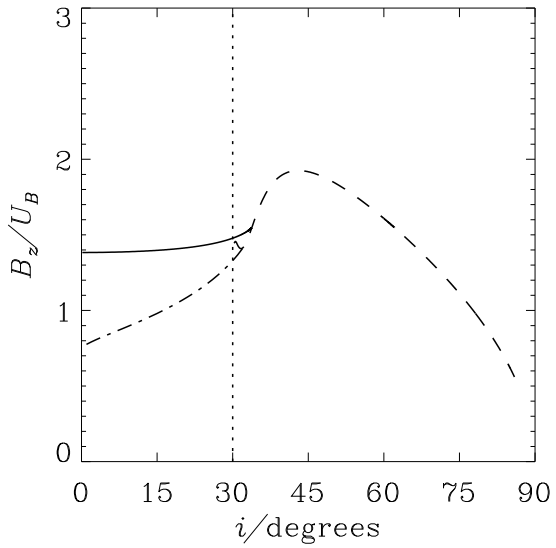

Figure 5

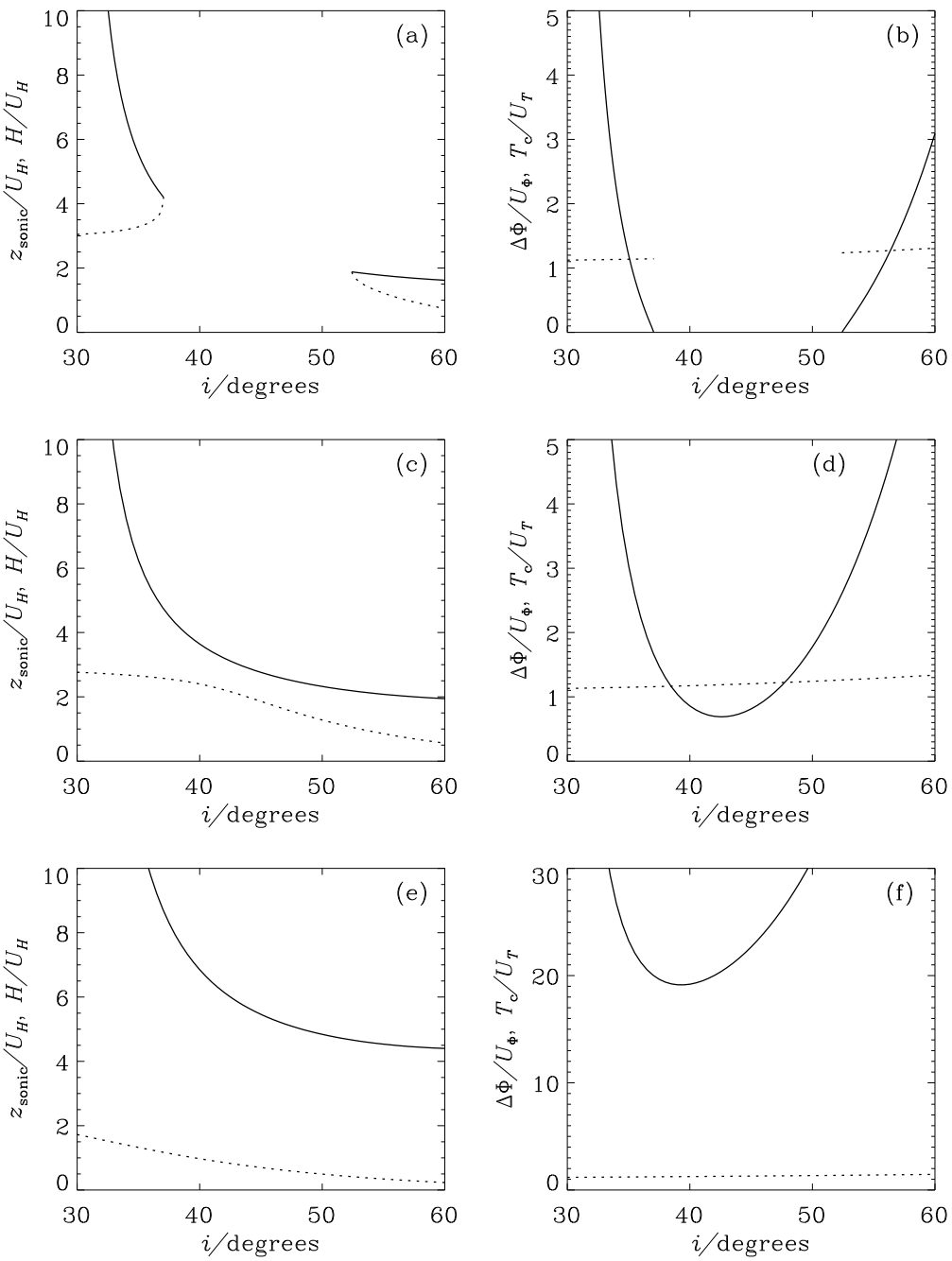

Figure 6

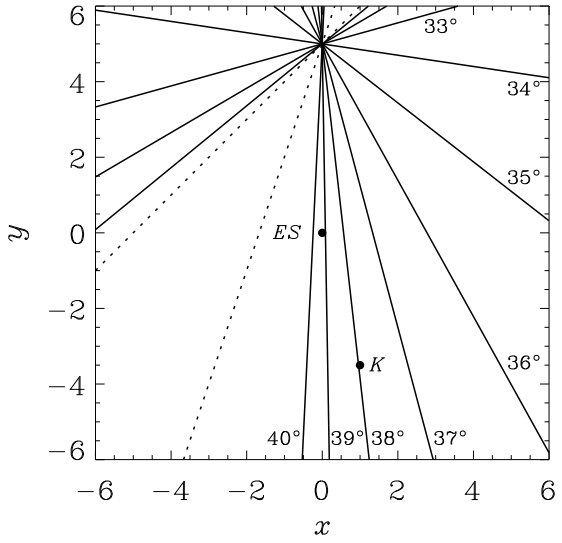

Figure 7

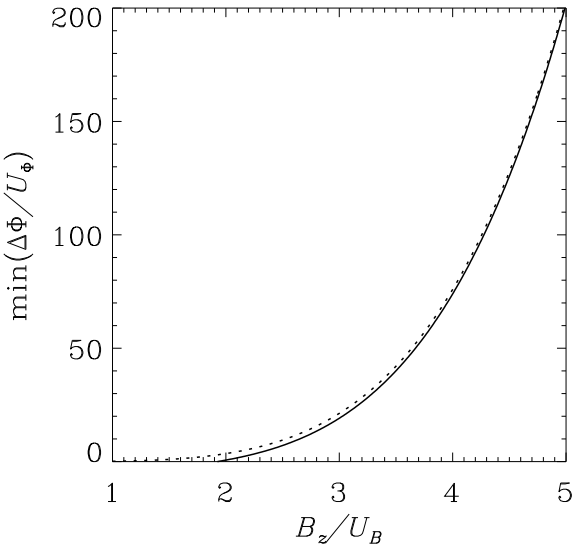

Figure 8